Probabilistic simulation of mesoscopic quantum paradoxes

M. D. Reid[1], B. Opanchuk[1], L. Rosales-Zárate[1] & P. D. Drummond[1]

[1]*Centre for Atom Optics and Ultrafast Spectroscopy, Swinburne University of Technology, Melbourne 3122, Australia*

Mesoscopic quantum paradoxes, like the famous Schrödinger cat, are increasingly accessible to experiment. While testing quantum mechanics under such conditions is an important challenge, the computation of quantum predictions in these states is notoriously difficult owing to exponential complexity. The most straightforward approach of using probabilistic or "Monte-Carlo" sampling was thought by Feynman and others to be impossible, due to the famous Bell inequality. It is an open question whether probabilistic simulations of these states can be carried out, and what are their error properties. Here we resolve this question by carrying out direct probabilistic simulations of several quantum paradoxes using a digital computer. We have treated multipartite Bell violations for up to 60 qubits, similar to those generated in photonic and ion-trap experiments, both with and without decoherence. Our results demonstrate that quantum paradoxes are directly accessible to probabilistic sampling methods, and we analyze the scaling properties of sampling errors. We anticipate that our results may provide a starting point for the development of more sophisticated computational tools, both for testing quantum theory at the boundary of the quantum and classical worlds, and for quantum engineering of new technologies that exploit this science.

The possibility of macroscopic entanglement[1] of quantum states has led to many conceptual problems[2]. In order to understand this limit, Feynman asked: *"Can quantum systems be probabilistically simulated by a classical computer?"*[3]. His answer was *"If ... there's no hocus-pocus, the answer is certainly, No!"*. The argument rested on the key assumption that violations of physically accessible Bell inequalities[4] could not be treated using probability distributions. Here we give counter-examples to this claim, through direct simulation of Bell's inequality violations.

What is the technique that allows these probabilistic simulations of Bell violations? We simulate quantum ensemble *averages*, not each individual observation. To achieve this, we employ the positive phase-space distributions of quantum optics[5–8] for our calculations. These have statistical moments which correspond to those measured in Bell violations. We generate phase-space distributions for a number of quantum states used to investigate quantum entanglement and Bell inequalities. Our methods are applied to states of the type generated with both the photonic and ion-trap experiments. We demonstrate a clear violation of a Bell inequality in every case, showing the failure of any local hidden-variable theory.

A Bell inequality is a constraint on observable correlations of a physical system that obeys a local hidden variable theory (LHV)[4,9]. This is a classical theory where measurements by two spatially separated observers (say, Alice and Bob) are obtained from random samples of a parameter λ. The measured values are functions of local detector settings and the hidden parameter λ. Thus, the value observed by Alice with detector setting a is $A(a,\lambda)$, and similarly for Bob. All

correlations are obtained from a probabilistic calculation of form:

$$\mathbf{C}(X,Y) = \int_{\Lambda} X(\lambda,a)Y(\lambda,b)P(\lambda)d\lambda \tag{1}$$

Here $X(\lambda,a)$ and $Y(\lambda,b)$ are experimental values, usually encoded as either 1 or -1 in a binary experiment. These assumptions lead to inequalities that any LHV correlations must satisfy. Quantum mechanics is known to violate these inequalities. But can one simulate these violations using probabilistic methods *equivalent* to quantum mechanics? Here we report probabilistic simulations of Bell inequality violations for polarized photons (Fig. 1), as in the seminal experiments of Clauser[9], Aspect et al.[10] and Zeilinger et al.[11], where:

$$|\psi\rangle = \frac{1}{\sqrt{2}}\left[|0\rangle|1\rangle|0\rangle|1\rangle + |1\rangle|0\rangle|1\rangle|0\rangle\right]. \tag{2}$$

To achieve this result, we use the positive P-representation[6,8], which is an exact expansion of an arbitrary density matrix of bosons with a positive probability distribution $P(\boldsymbol{\alpha},\boldsymbol{\beta})$. In terms of this general distribution, the correlation of quantum counts $\hat{n}_i = \hat{a}_i^\dagger \hat{a}_i$ at different locations is:

$$\langle \hat{n}_i \ldots \hat{n}_j \rangle = \int n_i \ldots n_j P(\boldsymbol{\alpha},\boldsymbol{\beta}) d^{2M}\boldsymbol{\alpha} d^{2M}\boldsymbol{\beta} \tag{3}$$

where $n_i \equiv \alpha_i\beta_i$. There is a remarkable similarity between the hidden variable theory (1) of Bell, and the positive-P formula (3) for quantum correlations. However, the positive-P representation *can* be used even for states that violate a Bell inequality[12]. The crucial reason for this difference is due to the different quantities sampled in the correlations. The fundamental observables in Bell's case, of form $X(\lambda,a)$, are equal to actual observed real numbers — i.e., $(0,1,\ldots)$ for photon

counts. The corresponding observables in the positive-P case, of form $n(\boldsymbol{\alpha}, \boldsymbol{\beta})$, are complex numbers whose *mean* values and correlations correspond to observable means and correlations. The results of the simulations are shown in Fig. 1, with the details in the Supplementary Methods online. These indicate a clear violation of a Bell inequality in both the two-particle case ($N = 1$) and the four-particle case ($N = 2$) which has also been observed experimentally[13].

To understand the ultimate scaling properties of probabilistic sampling methods, we have also simulated higher order correlations that violate multipartite Bell inequalities. These are found in quantum states that display Bell violations with M observers, not just two. The most well-known examples are the multimode entangled Greenberg-Horne-Zeilinger-Mermin (GHZM) states[14,15], corresponding to "Schrödinger Cat" states. We therefore considered GHZM states which describe M spin-$\frac{1}{2}$ particles or qubits:

$$|\Phi\rangle = \frac{1}{\sqrt{2}}\left(|\uparrow \ldots \uparrow\rangle + e^{i\phi}|\downarrow \ldots \downarrow\rangle\right). \tag{4}$$

Here $|\uparrow\rangle$ and $|\downarrow\rangle$ denote spin-up or spin down particles in the z-direction. As well as being of deep significance in quantum physics, such mesoscopic states have been generated in recent ion-trap experiments[16–18]. Quantum paradoxes are obtained on measuring an operator $\hat{A}$ which is defined as a linear combination of 2^M distinct M-th order correlation functions:

$$\hat{A} = \prod_{j=1}^{M}\left(\hat{\sigma}_x^j + is_j\hat{\sigma}_y^j\right)e^{-is_j\theta_j}. \tag{5}$$

For odd M we follow Mermin[15] and take $\phi = -\pi/2$, $s_j = 1$ and $\theta_j = 0$. For even M we

follow Ardehali[19] and take $\phi = \pi$, $s_j = -1$ and $\theta_j = 0$ for $j < M$, $s_M = 1$, $\theta_M = -\pi/4$. Genuine multipartite Bell violations are known to exist for these states, which imply that the observed correlations cannot be explained by a nonlocality shared among $M - 1$ or fewer qubits. To test for genuine multipartite Bell nonlocality, we adopt the hybrid local-nonlocal LHV model introduced by Svetlichny[20] and Collins et al.[21]. In order to simulate the Bell violation for these multipartite states, we use the SU(2)-Q distribution, which is well-suited to this type of Hilbert space[5,22].

The difference between the positive-P and SU(2)-Q representation, compared to an LHV, can be illustrated by considering the case of $M = 2$, where simplifying the Ardehali inequality will give rise to the corresponding quantum mechanical expectation value:

$$F = -\langle \hat{\sigma}_x^1 \hat{\sigma}_x^2 \rangle + \langle \hat{\sigma}_y^1 \hat{\sigma}_y^2 \rangle. \tag{6}$$

The correlation between real parts of the values of two factors for one of the terms is plotted in Fig. 2a and 2c, and the correlation between the two terms of (6) is plotted in Fig. 2b and 2d. Note that neither of the representations limits the values of $\mathrm{Re}\,\sigma_x^1$ and $\mathrm{Re}\,\sigma_x^2$ to the range $[-1, 1]$, as would happen in an LHV. This essential feature means that Bell's theorem does not limit our results, because the sampled values are not the same as their physical eigenvalues. This property of having a different apparent range from the operator eigenvalues is also shared by the theory of "weak" measurements[23]. Other examples of quantum correlations have been treated using these methods, including quantum solitons[24], interacting quantum fields[25] equivalent to $\sim 10^6$ qubits and the Dicke superfluorescence model[26], although no previous Bell violations were reported. These simulated correlations are in general agreement with experimental observations[27].

The state (4) can be readily sampled using probabilistic random number generators together with the Q-function (details can be found in Supplementary Methods online). These samples can be used to calculate required expectation values (Fig. 3a). In the graph, the red dashed line is the minimum correlation required to demonstrate a Bell violation. Since the calculation is essentially a parallel one, we employed graphical processor unit (GPU) technology to calculate many samples in parallel, with a number of qubits ranging from $M = 2$ to $M = 60$. This corresponds to measurement of a quintillion (10^{18}) distinct sixtieth order correlation functions. Bell violations were verified in all cases, while genuine multipartite violations of LHV requiring all M observers to participate, with $F_{sample}/F_{QM} > 1/\sqrt{2}$, were verified for $M < 50$.

To understand the source of sampling errors, we investigated the scaling of errors with system-size for *single* measurements of a low-order spin correlation (Fig. 3b), in addition to the exponentially large numbers of measurements in the expectation values F. As an example of low-order correlation we have chosen the total number of "spin-ups" $N = \langle \sum_{j=1}^{M} (\hat{\sigma}_z^j + 1)/2 \rangle$. Low-order correlations were easily calculated with decreasing sampling errors as M increases. This explains why low order correlations could be efficiently sampled in previous work, for much larger Hilbert spaces than the ones studied here.

In contrast to this, high-order correlations showed exponentially increasing sampling error. The relative error in F scales as $2^{M/3}$, meaning that the time taken at constant error scales as $2^{2M/3}$. Surprisingly, probabilistic sampling scales more favorably than experiment, which would take time in proportion to 2^M, owing to the exponentially large number of measurements needed.

The increased efficiency of computational sampling is caused by the exponentially large number of measurements that are calculated in parallel in the phase-space simulations. This more than offsets the large number of samples required.

Experimental measurements of such high-order correlations are limited due to noise and decoherence, which is an important issue in the observation of mesoscopic quantum effects[28]. The experimentally observed magnetic field noise found in ion-trap experiments can be easily added using a simple model. Following Monz et al.[18], we assume a delta-correlated noise such that $\langle \Delta E(t) \Delta E(t') \rangle = \Delta E_0^2 \delta(t - t')$, with an interaction Hamiltonian of the form:

$$\hat{H} = \frac{\Delta E(t)}{2} \sum_{j=1}^{M} \hat{\sigma}_z^j. \tag{7}$$

By analyzing operator correspondences in the Heisenberg picture, we find that this can also be readily simulated. This was achieved by multiplying an independent noise term $\exp(i\epsilon M \zeta_j)$ by the value corresponding to the operator A in each of the samples after every time step Δt. Here $\epsilon = \Delta E_0 \sqrt{\Delta t}/\hbar$ defines the speed of the decoherence, and ζ_j is a Gaussian random number such that $\langle \zeta_j \zeta_{j'} \rangle = \delta_{jj'}$. This is shown in Fig. 4, which demonstrates the experimentally observed quadratic super-decoherence as M increases.

We see from the present results that while higher order correlations in GHZM states *can* be simulated, they require many samples to reduce errors to acceptable levels. This result is not completely unexpected. Higher-order correlations are often associated with isolated quantum states,

which effectively become “needles in a hay-stack” in large Hilbert spaces. Universal digital quantum computers are expected to become useful to overcome this problem[29]. However, these are currently limited in size to around 6 qubits or less[30]. Scientifically, to test quantum theory it is also important to obtain quantum predictions using methods that do not inherently rely on quantum mechanics being correct.

In summary, it is not impossible to use probabilistic digital algorithms to simulate mesoscopic quantum paradoxes comparable to those found in current experiments. Such quantum technologies are already finding applications in quantum logic based encryption, atomic clocks and interferometers. Digital simulations could have a direct application to the design and implementation of these technologies, as well as providing quantum predictions for fundamental tests of quantum physics.

1. Einstein, A., Podolsky, B. & Rosen, N. Can Quantum-Mechanical Description of Physical Reality Be Considered Complete? *Phys. Rev.* **47**, 777–780 (1935).

2. Schrödinger, E. Die gegenwärtige Situation in der Quantenmechanik. *Naturwissenschaften* **23**, 807–812 (1935).

3. Feynman, R. P. Simulating physics with computers. *Int. J. Theor. Phys.* **21**, 467–488 (1982).

4. Bell, J. S. On the Einstein-Podolsky-Rosen paradox. *Physics* **1**, 195–200 (1964).

5. Husimi, K. Some Formal Properties of the Density Matrix. *Proc. Phys. Math. Soc. Jpn.* **22**, 264–314 (1940).

6. Drummond, P. D. & Gardiner, C. W. Generalised P-representations in quantum optics. *J. Phys. A: Math. Gen.* **13**, 2353–2368 (1980).

7. Hillery, M., O'Connell, R. F., Scully, M. O. & Wigner, E. P. Distribution functions in physics: Fundamentals. *Phys. Rep.* **106**, 121–167 (1984).

8. Gardiner, C. W. & Zoller, P. *Quantum Noise* (Springer, 2004), 4th edn.

9. Clauser, J. F., Horne, M., Shimony, A. & Holt, R. Proposed Experiment to Test Local Hidden-Variable Theories. *Phys. Rev. Lett.* **23**, 880–884 (1969).

10. Aspect, A., Dalibard, J. & Roger, G. Experimental Test of Bell's Inequalities Using Time-Varying Analyzers. *Phys. Rev. Lett.* **49**, 1804–1807 (1982).

11. Weihs, G., Jennewein, T., Simon, C., Weinfurter, H. & Zeilinger, A. Violation of Bell's Inequality under Strict Einstein Locality Conditions. *Phys. Rev. Lett.* **81**, 5039–5043 (1998).

12. Drummond, P. D. Violations of Bell's Inequality in Cooperative States. *Phys. Rev. Lett.* **50**, 1407–1410 (1983).

13. Howell, J., Lamas-Linares, A. & Bouwmeester, D. Experimental Violation of a Spin-1 Bell Inequality Using Maximally Entangled Four-Photon States. *Phys. Rev. Lett.* **88**, 030401 (2002).

14. Greenberger, D. M., Horne, M. & Zeilinger, A. *Bell's Theorem, Quantum Theory and Conceptions of the Universe* (Springer, 1989).

15. Mermin, N. D. Extreme quantum entanglement in a superposition of macroscopically distinct states. *Phys. Rev. Lett.* **65**, 1838–1840 (1990).

16. Rowe, M. A. *et al.* Experimental violation of a Bell's inequality with efficient detection. *Nature* **409**, 791–794 (2001).

17. Leibfried, D. *et al.* Creation of a six-atom 'Schrödinger cat' state. *Nature* **438**, 639–642 (2005).

18. Monz, T. *et al.* 14-Qubit Entanglement: Creation and Coherence. *Phys. Rev. Lett.* **106**, 130506 (2011).

19. Ardehali, M. Bell inequalities with a magnitude of violation that grows exponentially with the number of particles. *Phys. Rev. A* **46**, 5375–5378 (1992).

20. Svetlichny, G. Distinguishing three-body from two-body nonseparability by a Bell-type inequality. *Phys. Rev. D* **35**, 3066–3069 (1987).

21. Collins, D., Gisin, N., Popescu, S., Roberts, D. & Scarani, V. Bell-Type Inequalities to Detect True n-Body Nonseparability. *Phys. Rev. Lett.* **88**, 170405 (2002).

22. Arecchi, F., Courtens, E., Gilmore, R. & Thomas, H. Atomic Coherent States in Quantum Optics. *Phys. Rev. A* **6**, 2211–2237 (1972).

23. Aharonov, Y., Albert, D. & Vaidman, L. How the result of a measurement of a component of the spin of a spin-1/2 particle can turn out to be 100. *Phys. Rev. Lett.* **60**, 1351–1354 (1988).

24. Drummond, P. D., Shelby, R. M., Friberg, S. R. & Yamamoto, Y. Quantum solitons in optical fibres. *Nature* **365**, 307–313 (1993).

25. Deuar, P. & Drummond, P. D. Correlations in a BEC Collision: First-Principles Quantum Dynamics with 150 000 Atoms. *Phys. Rev. Lett.* **98**, 120402 (2007).

26. Altland, A. & Haake, F. Equilibration and macroscopic quantum fluctuations in the Dicke model. *New J. Phys.* **14**, 073011 (2012).

27. Jaskula, J.-C. *et al.* Sub-Poissonian Number Differences in Four-Wave Mixing of Matter Waves. *Phys. Rev. Lett.* **105**, 190402 (2010).

28. Brune, M. *et al.* Observing the Progressive Decoherence of the "Meter" in a Quantum Measurement. *Phys. Rev. Lett.* **77**, 4887–4890 (1996).

29. Lloyd, S. Universal Quantum Simulators. *Science* **273**, 1073–1078 (1996).

30. Lanyon, B. P. *et al.* Universal digital quantum simulation with trapped ions. *Science* **334**, 57–61 (2011).

Acknowledgements L. E. C. R. Z. acknowledges financial support from CONACYT, Mexico. P. D. D. thanks the Australian Research Council for funding via a Discovery grant, and for discussions with P. Deuar.

Supplementary Information

***** Supplementary Methods

In this supplementary information, we give the technical details of the probability distributions and sampling techniques used to obtain the data in the main paper.

Bell inequalities. The sampling of the Bell inequalities is performed using the positive-P representation of the correlated multi-photon target state. Here we consider correlated states with N photon pairs, which are described by the following ideal quantum state:

$$|N\rangle = \frac{\left(a_{1+}^{\dagger}a_{2+}^{\dagger} + a_{1-}^{\dagger}a_{2-}^{\dagger}\right)^{N}|0\rangle}{N!\left(N+1\right)^{1/2}}, \tag{8}$$

where N is the number of photon pairs. These states are generated in certain types of optical parametric down-conversion experiments, and have been studied by several different groups. We define the intensity correlations to be $G^{IJ}(\gamma, N) = \langle N|\hat{A}^{I}(1, \boldsymbol{a}_1)\hat{A}^{J}(\gamma, \boldsymbol{a}_2)|N\rangle$, where γ is a linear combination parameter related to a polarizer angle, and auxiliary functions are introduced so that:

$$\hat{A}^{J}(\gamma, \hat{\boldsymbol{a}}_k) = \left(\sqrt{\gamma}\hat{a}_{k-}^{\dagger} + \sqrt{1-\gamma}\hat{a}_{k+}^{\dagger}\right)^{J}\left(\sqrt{\gamma}\hat{a}_{k-} + \sqrt{1-\gamma}\hat{a}_{k+}\right)^{J}, \tag{9}$$

$$\hat{A}^{J}(\infty, \hat{\boldsymbol{a}}_k) =: \left(\hat{a}_{k-}^{\dagger}\hat{a}_{k-} + \hat{a}_{k+}^{\dagger}\hat{a}_{k+}\right)^{J} : . \tag{10}$$

Tthe standard two-particle CHSH form of Bell's inequality given by Clauser, Horne, Shimony and Holt, is especially important, as it gives classical limits to the expected correlation for the above experiment:

$$\mathbf{C}[A(a), B(b)] + \mathbf{C}[A(a), B(b')] + \mathbf{C}[A(a'), B(b)] - \mathbf{C}[A(a'), B(b')] \leq 2\,. \tag{11}$$

More generally, for N photon pairs, the Bell-type inequality is then known to be of the form:

$$\Delta(\theta) = 3g(\theta) - g(3\theta) - 2 \leq 0, \tag{12}$$

where

$$g_N^J(\theta) = G^{JJ}(\cos^2\theta, N)/G^{JJ}(\infty, N). \tag{13}$$

While this expression generalizes the usual CHSH and Bell expressions to a multi-particle form, the quantum mechanical prediction for g_N^J has especially simple form of $g_N^N(\theta) = \cos^{2N}\theta$ for the cases $J = N$, $N = 1, 2$ which we have simulated. This gives violations of

$$\Delta_{1\,\mathrm{pair}}(\theta) = 3\cos^2\theta - \cos^2 3\theta - 2, \tag{14}$$

for the two particle case, which corresponds to the usual two-particle experiment originally proposed by Bell. For the four-particle case one finds that:

$$\Delta_{2\,\mathrm{pairs}}(\theta) = 3\cos^4\theta - \cos^4 3\theta - 2. \tag{15}$$

In all cases, the corresponding photonic system is a four-mode state $|N\rangle$, which has the corresponding positive-P distribution

$$P(\boldsymbol{\alpha},\boldsymbol{\beta}) = \left\{ \frac{\left|\left(\beta_{1+}+\alpha_{1+}^{*}\right)\left(\beta_{2+}+\alpha_{2+}^{*}\right)+\left(\beta_{1-}+\alpha_{1-}^{*}\right)\left(\beta_{2-}+\alpha_{2-}^{*}\right)\right|^{2N}}{(2\pi)^{8}\left(N+1\right)\left(N!\right)^{2}2^{4N}} \right\} \exp\left(-\frac{|\boldsymbol{\alpha}|^{2}+|\boldsymbol{\beta}|^{2}}{2}\right). \tag{16}$$

This distribution exists and has a positive, probabilistic behavior for all values of N. We sampled this distribution by transforming to a form where we could use the well-known von Neumann rejection algorithm, combined with an underlying lambda-distribution. The exact results are plotted in Fig. 1, together with the probabilistic sampling results.

GHZM states and SU(2)-Q representation To handle systems with many distinct observers — known as multipartite systems — we found it most efficient to use a representation that was optimized for treating quantum binary states or qubits. These are the SU(2) coherent states and the corresponding positive Q-function. For an M-mode system the un-normalized SU(2) coherent states are defined as:

$$|\mathbf{z}\rangle = e^{\hat{S}^{\dagger}\cdot\mathbf{z}}\,|0\rangle = \prod_{j=1}^{M}\left[|0\rangle_{j}+z_{j}\,|1\rangle_{j}\right]. \tag{17}$$

The SU(2) Q-function is the expectation value of the density operator over the SU(2) coherent states, and is defined explicitly in a normalized form as:

$$Q(\mathbf{z}) = \left[\prod_{j=1}^{M}\frac{2}{\pi\left(1+|z_{j}|^{2}\right)^{3}}\right]\langle\mathbf{z}\|\,\hat{\rho}\,\|\mathbf{z}\rangle\,. \tag{18}$$

For the GHZ states (4), the SU(2) Q-function is easily computed using the orthogonality of the spin basis. This leads to a positive distribution for a GHZ state with M sites:

$$Q(\mathbf{z}) = \frac{1}{2}\prod_{j=1}^{M}\frac{2}{\pi\left(1+|z_{j}|^{2}\right)^{3}}\left|\prod_{j=1}^{M}z_{j}+e^{-i\phi}\right|^{2}. \tag{19}$$

In this case the sampling was again carried out by using a von Neumann rejection algorithm combined with an inverse cumulative distribution which was sampled exactly.

The expectation value of the operator $\hat{A}$ (5) which gives the multi-partite Bell violations in terms of the SU(2)-Q function is also able to be computed, using the properties of the spin operators. It is given by:

$$\langle\Phi|\hat{A}|\Phi\rangle \;\; = \;\; \int d\boldsymbol{z}\, Q(\mathbf{z}) \prod_{j=1}^{M} \frac{3\left((1+s_j)z_j^* + (1-s_j)z_j\right) e^{-is_j\theta_j}}{1+|z_j|^2}. \tag{20}$$

The expectation of the number of "spin-ups" can be shown to be

$$\langle\Phi| \sum_{j=1}^{M} \frac{\hat{\sigma}_z^j + 1}{2} |\Phi\rangle = \int d\boldsymbol{z}\, Q(\mathbf{z}) \sum_{j=1}^{M} \left(\frac{2|z_j|^2 - 1}{1+|z_j|^2} \right). \tag{21}$$

As described in the main text, for odd M we follow Mermin [15] and take $\phi = -\pi/2$, $s_j = 1$ and $\theta_j = 0$. The value of interest in this case is $F = \mathrm{Im}\langle\Phi|\hat{A}|\Phi\rangle$, which is limited to $2^{(M-1)/2}$ by any LHV, but has a quantum mechanical (QM) expectation of 2^{M-1}. For even M we follow Ardehali [19] and take $\phi = \pi$, $s_j = -1$ and $\theta_j = 0$ for $j < M$, $s_M = 1$, $\theta_M = -\pi/4$. The value of interest is $F = \left|\mathrm{Re}\langle\Phi|\hat{A}|\Phi\rangle\right| + \left|\mathrm{Im}\langle\Phi|\hat{A}|\Phi\rangle\right|$ with a QM expectation of $2^{M-1/2}$. Here the LHV limit is $2^{M/2}$. Therefore, for any M we have a relative violation $2^{(M-1)/2}$.

This result is used to calculate the variance in the low-order correlations. All of these results were calculated using a numerical code that generates the samples, calculates the corresponding correlation function, and accumulates the result for averaging. In order to obtain

low enough sampling error to give the strong correlations needed to violate 60th order Bell inequalities, and show genuine multipartite Bell violations, we needed to use adequate numbers of samples. The results given here required 10^{12} samples, which were obtained using GPU multiprocessor technology. The results reported here required up to about 24 hours on four parallel GPU processors, each with 448 cores. The code for the simulations is available publicly at `http://github.com/Manticore/bellsim-letter`.

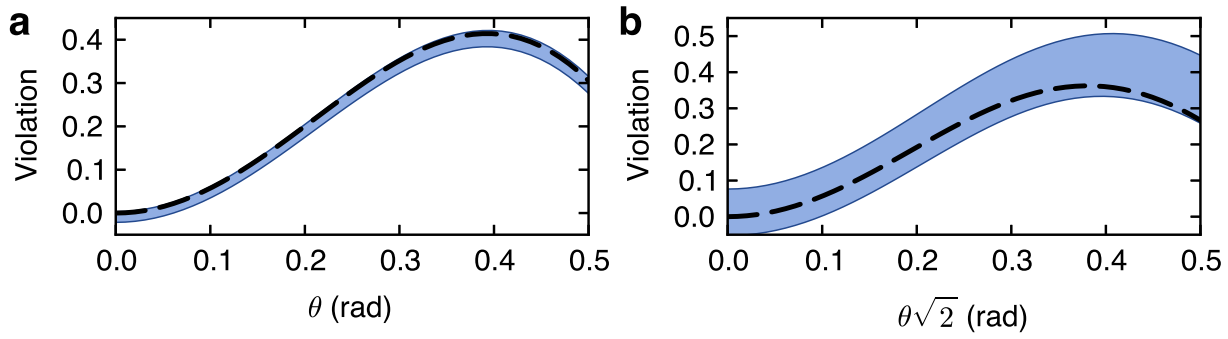

Figure 1 Bell violation. Simulated Bell violation Δ as a function of the relative polarizer angle θ for one (**a**) and two (**b**) photon pairs using the positive-P distribution with 2^{21} (**a**) and 2^{25} (**b**) samples. The filled area corresponds to the estimated error range around the mean of $\Delta(\theta)$ for the sampled state, while the dashed line is the exact quantum mechanical prediction of this value.

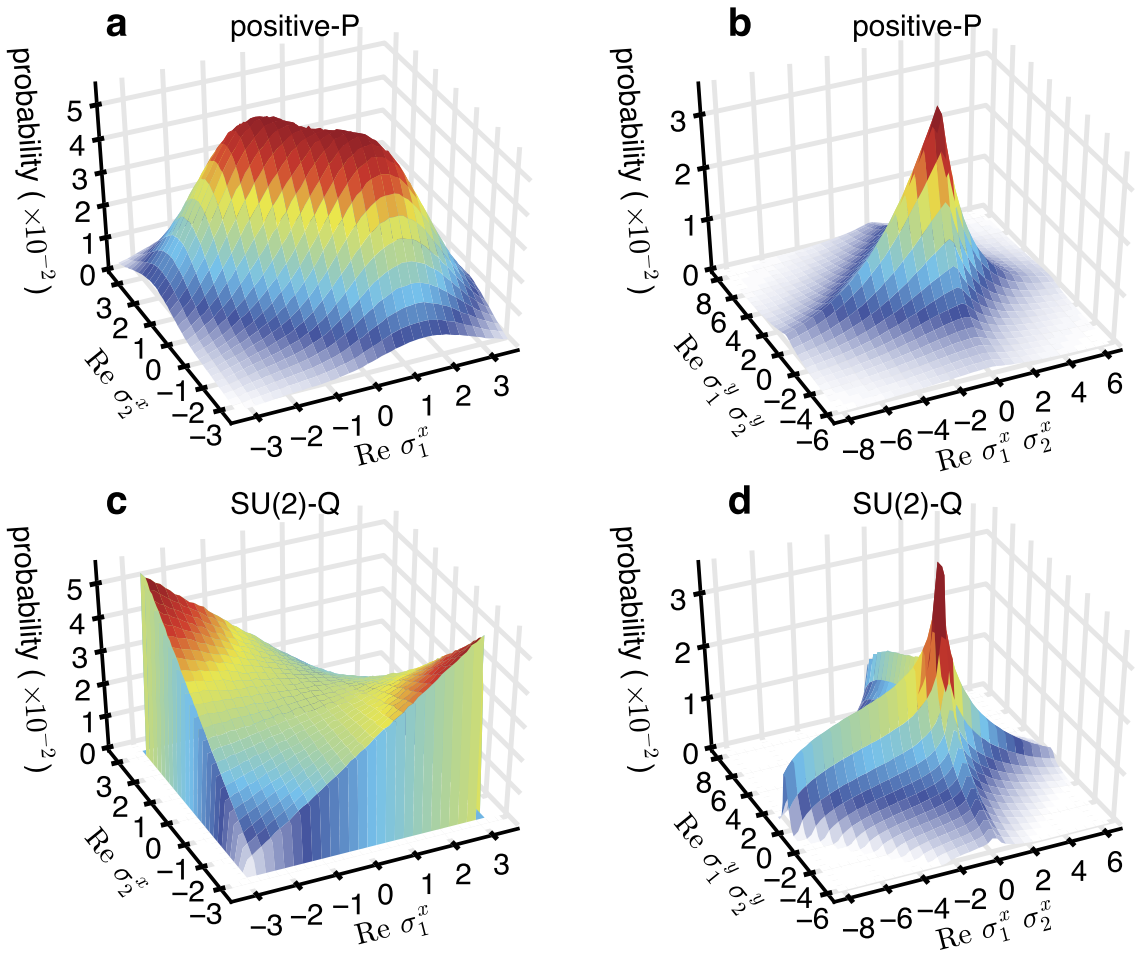

Figure 2 Spin moment correlations. Correlations for the different parts of the quantity (6), in case of positive-P (**a**, **b**) and SU(2)-Q (**c**, **d**) representations, 10^8 samples.

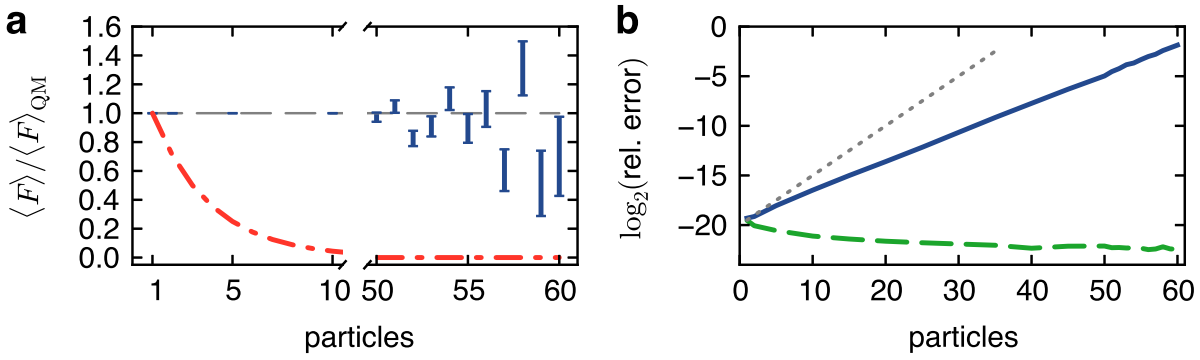

Figure 3 Violations for multi-particle GHZ states. **a**, Simulated Mermin violation using SU(2)-Q representation. The values of expectations and errors are normalized by the quantum mechanical prediction for the corresponding M. The horizontal grey dashed line gives the quantum prediction. The error bars show the sampled result and estimated sampling errors at each value of M. The red dash-dotted line is the LHV prediction, which gives a Bell violation when above this line. Genuine multipartite Bell violations occur for $F_{\mathrm{sample}}/F_{\mathrm{QM}} > 1/\sqrt{2}$. **b**, Relative errors for F (blue line) and first order correlation, or total number of "spin-ups" (green dashed line) using SU(2)-Q representation. The dotted reference line shows the point at which the sampling errors would give scaling properties as slow as an experimental measurement.

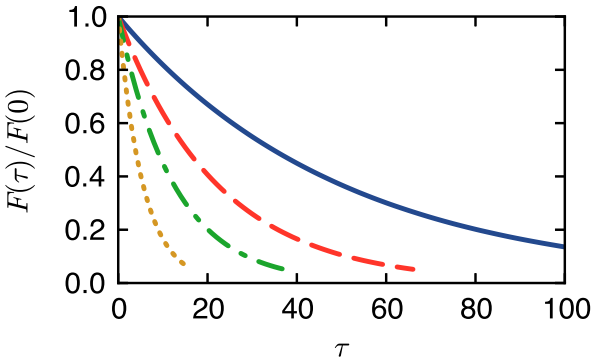

Figure 4 The effect of decoherence on measured quantities. Decay of the sampled quantity F after the application of the simple model of super-decoherence (7), for 2 (solid blue line), 3 (red dashed line), 4 (green dash-dotted line) and 6 (yellow dotted line) particles, with decoherence rate $\epsilon = 0.1$. The horizontal axis is the dimensionless time, $\tau = t/\Delta t$.